Towards 4D Photoacoustic Tomography

Felix Lucka[1], Marta Betcke[1], Simon Arridge[1], Ben Cox[2], Nam Huynh[2], Edward Zhang[2] and Paul Beard[2]

1) Department of Computer Science 2) Department of Medical Physics
University College London, WC1E 6BT London, UK

contact: f.lucka@ucl.ac.uk

Background & Project Overview

Photoacoustic Tomography (*PAT*) is an emerging *hybrid imaging* technique in which soft-tissue contrast induced by optical light waves gives rise to an acoustic wave propagation (**Fig. 1**). Measurements thereof can be used to reconstruct information for clinical and preclinical tasks with both high resolution and high contrast (**Fig. 2** & **3**). The long acquisition time of high-resolution PAT based on *Fabry Perot* (*FB*) interferometers forbids dynamic, real time 3D imaging (*4D PAT*). We try to overcome this limitation by combining recent advances in *spatio-temporal sub-sampling schemes*, *inverse problems* and *compressed sensing* with the development of tailored data acquisition systems (**Fig. 4**).

Sparse Variational PAT Inversion

We need to solve $f = GAp_0$, with G sub-sampling and A forward operator. As conventional approaches fail when used on sub-sampled data (cf. **Fig. 7**), we employ sparse variational regularization (e.g., *total variation*, *TV*),

$$\hat{p}_\lambda = \underset{p \geqslant 0}{\operatorname{argmin}} \tfrac{1}{2}\|f - GAp\|_2^2 + \lambda \mathcal{J}(p) \qquad (1)$$

enhanced by *Bregman iterations* (see Osher et al, 2005),

$$\hat{p}_\lambda^{k+1} = \underset{p \geqslant 0}{\operatorname{argmin}} \tfrac{1}{2}\|(f + b^k) - GAp\|_2^2 + \lambda \mathcal{J}(p)$$

$$b^{k+1} = b^k + f - GAp^{k+1}; \qquad b_1 = 0$$

to compensate the systematic bias of (1) (cf. **Fig 6**).

Implementation & Preliminary Results

To solve (1) by first order optimization such as *proximal gradient* or *(preconditioned) ADMM* schemes (cf. Burger et al., 2014), we need to evaluate A and A^*. Our implementation relies on a *k-space pseudo-spectral method* for 3D acoustic wave propagation (Treeby & Cox, 2010). We derived and tested an analytical and an explicit numerical representation of the adjoint A^* and utilized GPU computing to cope with the immense computational challenges.

Fig. 5, 6 & 7 show the evaluation of our methods with simulated data and demonstrate the potential of sparsity-based reconstructions from heavily sub-sampled data.

Fig. 8 & 9 show their application to experimental data of a static and a dynamic phantom. Various non-trivial difficulties such as developing pre-processing routines and improved forward models will have to be overcome to realize similar compression factors as in the simulations.

Spatio-Temporal Inversion

PAT data is continuously acquired. While using sparsity-based inversion on each short, sub-sampled stream of data (frame) individually can already significantly enhance the dynamic frame rate, full spatio-temporal schemes can also take advantage of the temporal redundancies of the data and lead to a better trade-off between spatial and temporal resolution.

Dependent on the underlying dynamics, different dynamic models will be implemented and tested in the future:

- *Low-rank* (+ sparsity) models for functional imaging with static anatomy.
- *Tracer uptake/kinetic models* for tracer-based imaging.
- *Perfusion models* for bolus tracking
- *Optical flow constraints* for joint image reconstruction and motion estimation.

Simultaneously, numerical and experimental phantoms will be developed to evaluate our results.

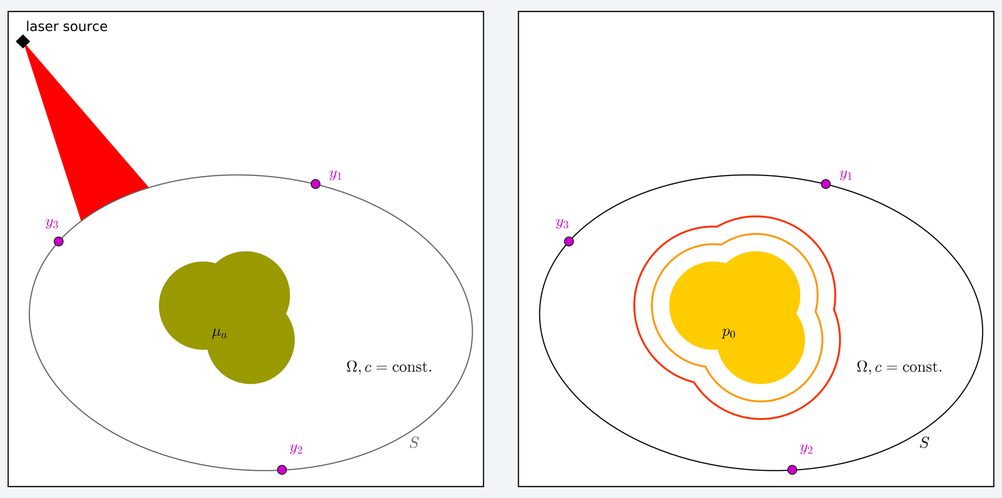

Fig. 1: In PAT, a short (ns) pulse of laser light is sent into biological tissue where it spreads until it is absorbed (μ_a, left picture) whereupon it creates a local increase in pressure which propagates to the surface as a broadband, ultrasonic pulse (p_0, right picture). If the amplitude of this signal is recorded over an array of sensors (y_i) at the tissue surface, p_0 and subsequently, μ_a can be reconstructed.

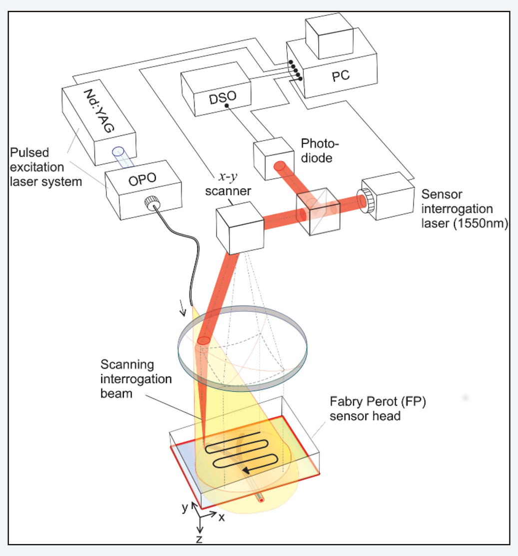

Fig. 2: Fabry Perot interferometers scan the acoustic signal with high spatial resolution and sensitivity (Zhang et al., 2008).

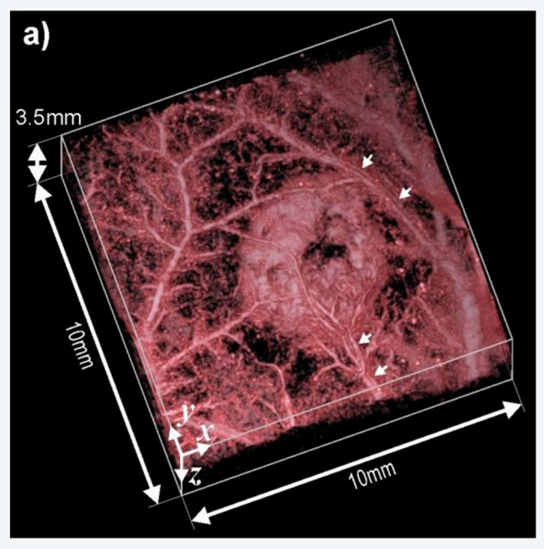

Fig. 3: *In vivo* PAT image of murine tumor vasculature; from Laufer et al., 2012.

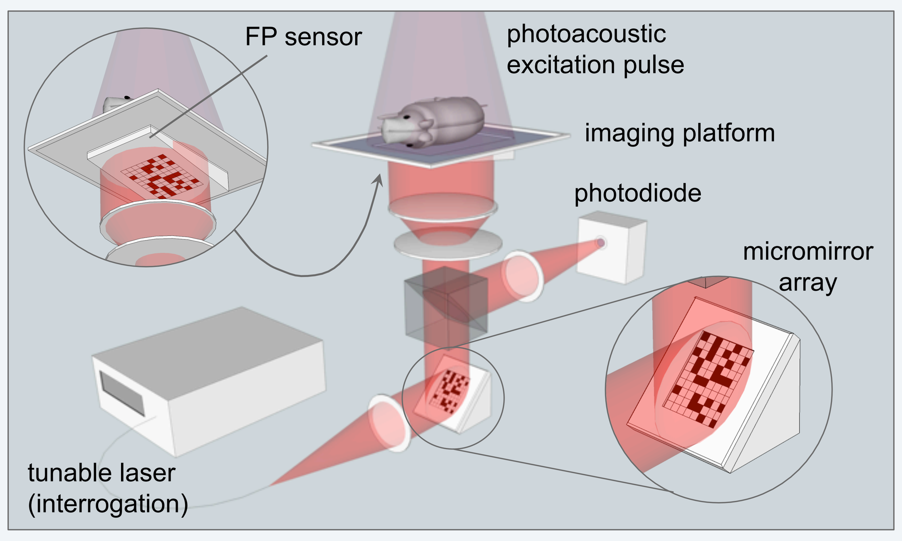

Fig. 4: Sketch of a "rice-camera"-like data acquisition system: Light from the interrogation laser is patterned by the micromirror array, reflected from the FB sensor, and focused into a single photodiode, see Huynh et al., 2014.

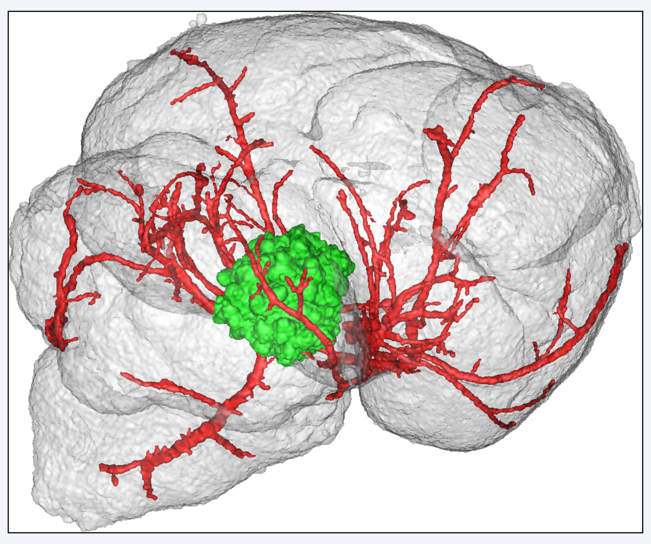

Fig. 5: Numerical phantom mimicking a scenario like in Fig. 3 for simulating the perfusion of vascular (red) and tumorous (green) brain tissue.

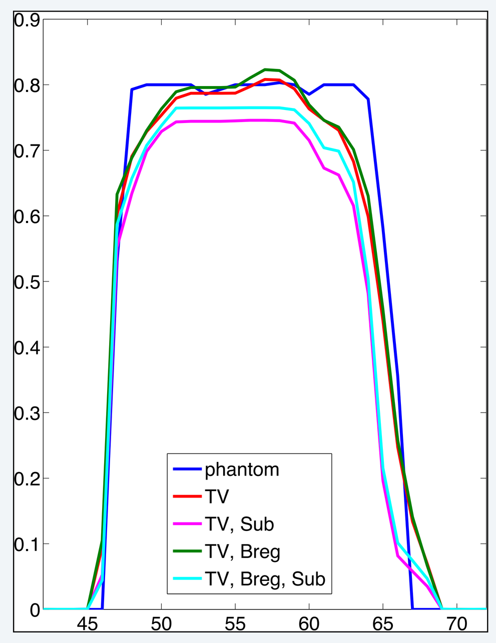

Fig. 6: X cross section (y=76,z=68) through different reconstructions.

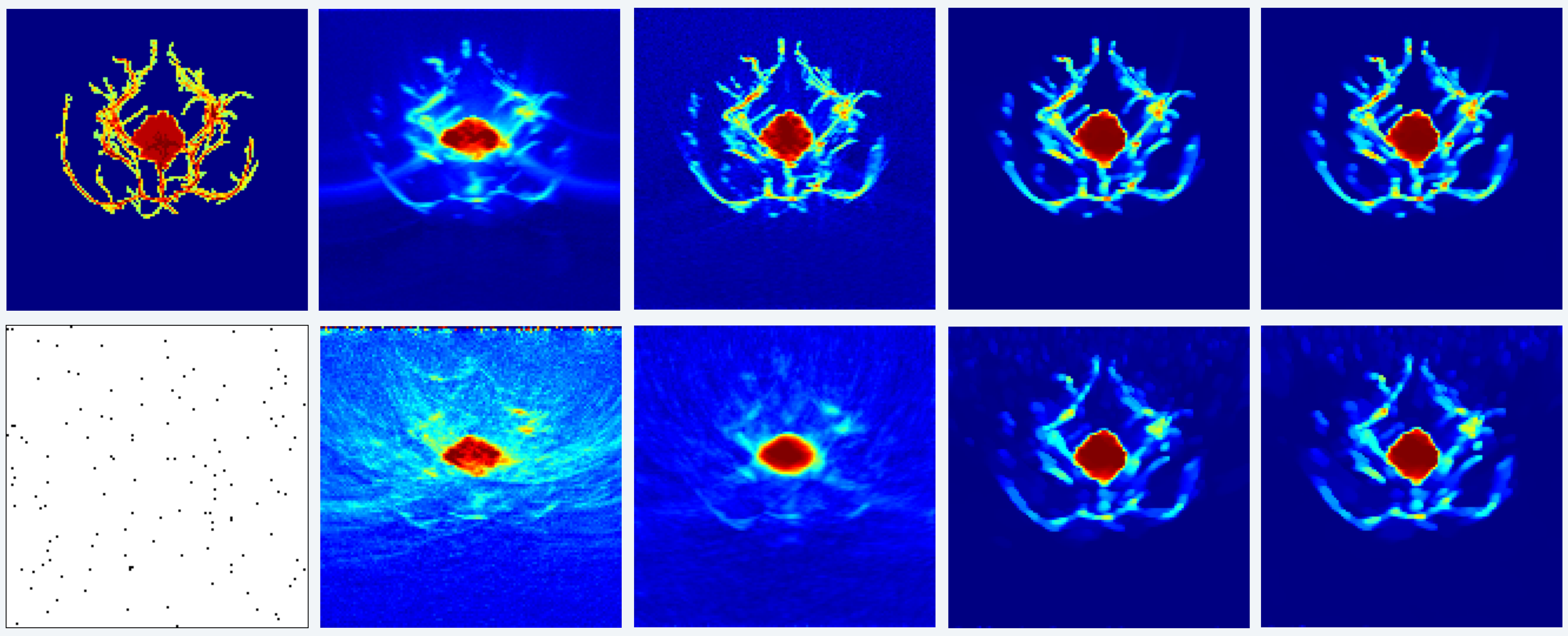

Fig. 7: Reconstructions of the phantom in Fig 5 (maximum intensity projection in the top right picture, size: 128^3 voxels) from full data and sub-sampled data consisting of a random subset of 0.78% of all scanning locations (left bottom image), which corresponds to a compression factor of 128. *Second column*: Standard time-reversal reconstruction technique (cf. Treeby & Cox, 2010) applied to the full (top) and sub-sampled (bottom) data. *Third column*: Corresponding pseudo inverse solution (i.e. (1) without regularization). *Fourth column*: TV regularization. *Fifth column*: Bregman iterations. For poster print, the contrast of the low intensities was enhanced by applying $sc(p) = p^{3/4}$ to the normalized intensities ($p \in [0, 1]$).

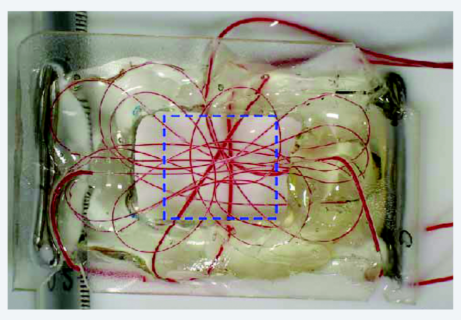

Fig. 8: Results for an experimental, blood-filled tube phantom (*left figure*, see Zhang et al., 2008). *Bottom row from left to right:* Picture of phantom, time-reversal solution, pseudo inverse and TV regularization.

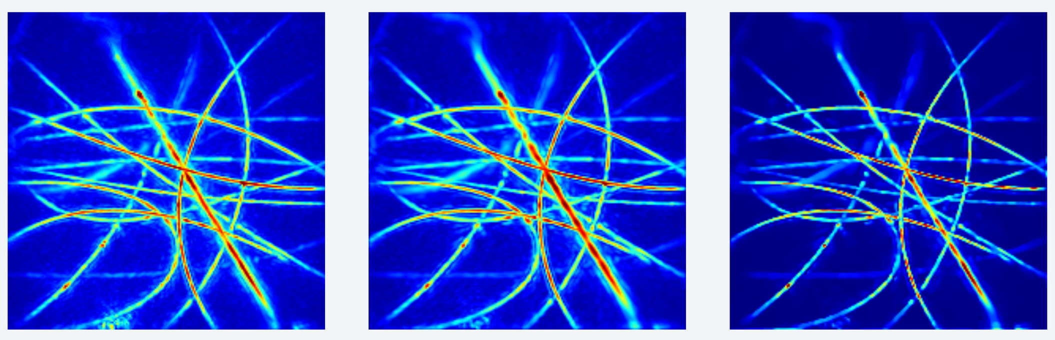

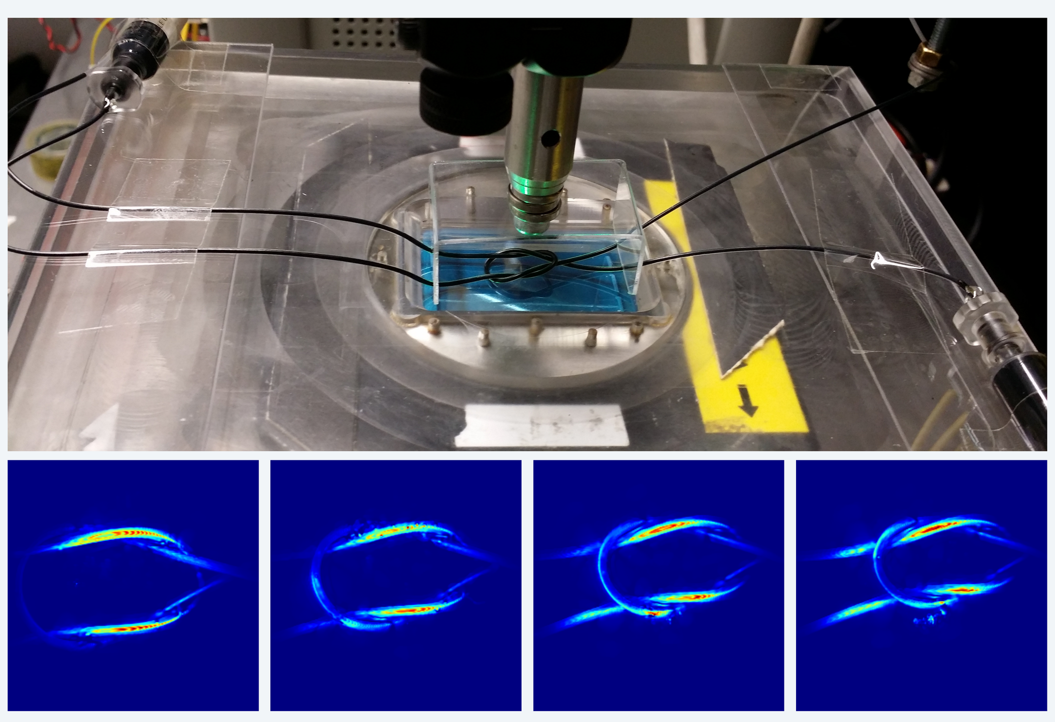

Fig. 9: Dynamic phantom: A knot of ink-filled tubes is pulled and measured in a stop-motion way in 45 frames (*top figure*). *Bottom figures:* TV regularized reconstructions for different time frames.

References & Acknowledgements

Burger, Sawatzky, Steidl, 2014. First Order Algorithms in Variational Image Processing, arXiv:1412.4237.

Huynh, Zhang, Betcke, Arridge, Beard Cox, 2014. Patterned interrogation scheme for compressed sensing photoacoustic imaging using a Fabry Perot planar sensor, *Proc. SPIE*, 8943.

Laufer, Johnson, Zhang, Treeby, Cox, Pedley, Beard, 2012. In vivo preclinical photoacoustic imaging of tumor vasculature development and therapy, *Journal of Biomedical Optics*, 17(5).

Osher, Burger, Goldfarb, Xu, Yin, 2006. An iterative regularization method for total variation-based image restoration, *Multiscale Modeling and Simulation*, 2(4).

Zhang, Laufer, Beard, 2008. Backward-mode multi-wavelength photoacoustic scanner using a planar fabry-perot polymer film ultrasound sensor for high-resolution three-dimensional imaging of biological tissues, *Applied Optics*, 47(4)

Treeby, Cox, 2010. k-Wave: MATLAB toolbox for the simulation and reconstruction of photoacoustic wave fields, *Journal of Biomedical Optics*, 2(15).

We gratefully acknowledge the support of NVIDIA Corporation with the donation of the Tesla K40 GPU used for this research.

UCL CENTRE FOR INVERSE PROBLEMS

EPSRC Engineering and Physical Sciences Research Council

cmic Centre for Medical Image Computing